Magnetic Resonance in Medicine 58:185–189 (2007)

Investigation of Human Cervical and Upper Thoracic Spinal Cord Motion: Implications for Imaging Spinal Cord Structure and Function

C.R. Figley[1] and P.W. Stroman[1–3]*

Spinal cord (SC) motion is thought to be the dominant source of error in current diffusion and spinal functional MRI (fMRI) methods. However, until now, such motion has not been well characterized in three dimensions. While previous studies have predominantly examined motion in the superior/inferior (S/I) direction, the foci of the present study were the anterior/posterior (A/P) and right/left (R/L) components of human cervical and upper thoracic SC motion. Cardiac-gated, turbofast low-angle shot (turbo-FLASH) cinematic MRI was employed at 3T to acquire images of the cord at 24 phases throughout the cardiac cycle. Time-dependent signal fluctuations within voxels adjacent to the cord/cerebrospinal fluid (CSF) interface were then used to measure SC motion, which was found to occur predictably as a function of cardiac activity. Cord movement was largest in the A/P direction, for which principal components of motion were calculated, thereby indicating consistent patterns of SC oscillation that can potentially be used to improve SC imaging. Magn Reson Med 58:185–189, 2007. © 2007 Wiley-Liss, Inc.

Key words: human; spinal cord; motion; magnetic resonance imaging; fMRI; DTI

Functional magnetic resonance imaging (fMRI) and diffusion-tensor imaging (DTI) have made significant contributions to our knowledge of human brain function, organization, and pathology (1,2), and have more recently been implemented in studies of the human spinal cord (SC) (3–8). Spinal fMRI was initially adapted from brain fMRI methods, but has since evolved to deal with the length and small cross-sectional area of the cord, as well as magnetic susceptibility effects resulting from its proximity to vertebrae (9–11). These improvements have permitted more detailed studies of SC activity in healthy and SC injured (SCI) populations (12–14), demonstrating the potential utility of spinal fMRI for both research and clinical applications. DTI has also been applied to the human SC in a small number of studies, and holds promise for noninvasively analyzing white matter connectivity and integrity (15). However, the sensitivity of these methods is compromised due to errors arising from SC motion (11,16–18), which has been observed in a number of studies (19–25) but has not yet been adequately characterized in terms of its timing, direction, and magnitude in three dimensions. The objective of this study is to more fully characterize cervical and upper thoracic SC motion by measuring it in the anterior/posterior (A/P) and right/left (R/L) directions throughout the cardiac cycle.

Early imaging studies of SC motion employed intraoperative ultrasonography, whereby motion was observed through saline-filled laminectomies. In this manner, oscillations of the human SC were found to occur consistently at the cardiac rate (19), and cord motion in a canine model was found to cease completely upon transection of the nerve roots and supporting vasculature (20). These experiments suggest that motion of the cord results, at least in part, from pulsatile arterial blood flow. In contrast, pioneering MRI investigations described motion of the human brain, cerebrospinal fluid (CSF), and SC under normal physiological conditions (21,22). Complete characterization of SC motion was not the focus of these studies, and even though motion was only measured in the superior/inferior (S/I) direction, the results suggest that momentum from the cerebral cortex (initiated by myocardial contraction, an arterial pulse wave, and increased cerebral blood volume) is conserved, resulting in amplified motion of the less massive brainstem and SC (21,25).

Physiological motion of the cord is problematic for spinal fMRI and DTI because both methods are rooted in discerning between small, voxelwise signal intensity changes while simultaneously striving for optimal spatial and temporal resolution. SC motion has not been accounted for substantively in most of the spinal fMRI or DTI studies to date, and though a small amount of motion may be tolerated, more sophisticated, motion-compensating methods will be required as future studies attempt to parse function and structure with increased resolution and sensitivity. Knowing that SC motion (19,20,24) and CSF flow (21,26) occur synchronously with arterial pulsations and/or the heartbeat, improvements to spinal DTI and fMRI have resulted from minimizing motion effects associated with cardiac activity. Cardiac gating during data acquisition has been shown to reduce errors in DTI (17,18) and improve the sensitivity of spinal fMRI (27). Also, improved sensitivity and reproducibility of spinal fMRI have been observed by including traces of the peripheral pulse, but not respiratory traces, in a general linear model (GLM) analysis (11).

The literature to date therefore demonstrates that a more detailed understanding of cord motion is necessary to improve the sensitivity and reliability of SC imaging. It is

[1]Centre for Neuroscience Studies, Queen's University, Kingston, Ontario, Canada.

[2]Department of Diagnostic Radiology, Queen's University, Kingston, Ontario, Canada.

[3]Department of Physics, Queen's University, Kingston, Ontario, Canada.

Grant sponsors: International Spinal Research Trust (UK); Canada Research Chairs Program.

*Correspondence to: Dr. P.W. Stroman, Department of Diagnostic Radiology, c/o Centre for Neuroscience Studies, 228 Botterell Hall, Queen's University, Kingston, Ontario, Canada K7L 3N6. E-mail: stromanp@post.queensu.ca

Received 28 September 2006; revised 10 February 2007; accepted 11 March 2007.

DOI 10.1002/mrm.21260
Published online in Wiley InterScience (www.interscience.wiley.com).

expected that this new information will assist DTI and fMRI in becoming reliable tools for research and clinical assessment of SC structure and function.

MATERIALS AND METHODS

Test Subjects

Ten healthy volunteers (five males and five females) were included in the study. The subjects ranged in age, weight, and height from 18 to 30 years (mean: 23 ± 4 years), 54 to 100 kg (mean: 70 ± 13 kg), and 1.57 to 1.91 m (mean: 1.71 ± 0.12 m), respectively. All volunteers were in good health, had no history of spinal injury, and provided informed consent prior to enrollment in the study. All experimental procedures were reviewed and approved by the Human Research Ethics Board at Queen's University.

Data Acquisition

All subjects were imaged while lying supine in a 3T whole-body MRI system (Magnetom Trio; Siemens, Erlangen, Germany). Uniform RF pulses were transmitted with a body coil, while a posterior neck coil and the upper elements of a spine phased-array coil were used as receivers. Initial localizer images were acquired in three planes to provide a position reference for subsequent imaging.

Examination of A/P SC motion was achieved with a cardiac-gated, gradient-echo, turbofast low-angle shot (turbo-FLASH) imaging sequence (TE/TR/flip = 2.03 ms/44.66 ms/60°, four averages, FOV = 200 × 200 mm^2, matrix = 192 × 192). Though image data were collected continuously from a single 3-mm-thick, mid-sagittal slice, the cinematic imaging (cine) pulse sequence retrospectively gated the data over the course of many peripheral pulses (2–3 min depending on heart rate). Thus, images with 1.04 × 1.04 mm^2 in-plane resolution (Fig. 1) were acquired at 24 phases throughout the cardiac cycle.

The imaging protocol used to measure R/L SC motion was similar to that employed for A/P motion (described above), except for slice orientation and positioning. Because the A/P curvature of the SC was quite pronounced in some subjects, the slice position was selected to span the midline of the SC over the greatest length possible. The S/I span was therefore variable across subjects.

Image data were collected over a large number of heartbeats, causing contributions from swallowing, respiration, or other potential sources of error to be averaged out due to cardiac asynchrony. Therefore, it is presumed that any motion observed in the data is periodic with the cardiac cycle. Also, given that each image was reconstructed from data acquired over a specific percentage of the cardiac cycle, minor fluctuations in intrasubject heart rates throughout scanning were inherently accounted for, and motion data were automatically normalized, which allowed the data to be compared and combined across subjects.

Analysis of SC Motion

The image data were analyzed using custom software written in MatLab® (The Mathworks Inc., Natick, MA, USA). On the first image in each series (i.e., the image acquired at peripheral systole), a seed point was manually selected on the interface between the cervical SC and CSF. An automated algorithm then tracked inferiorly, identifying voxels positioned on the cord/CSF interface by analyzing the signal intensities within a 5 × 5 voxel grid (Fig. 2), initially centered at the seed point. The signal intensity of each voxel indicated the relative proportion of cord and CSF it contained at a given phase of the cardiac cycle. Within the grid, voxels containing entirely CSF displayed the highest signal intensities, while those occupied by SC displayed the lowest intensities. The intensities were linearly normalized and shifted to values of zero and one, respectively, with intermediate intensities generated by voxels spanning the cord/CSF boundary. The cord/CSF ratio fluctuated in time within voxels lying along the interface and demonstrated cord motion with respect to cardiac phase. Temporal variations were observed in adjacent voxels across the interface, demonstrating that the cord/CSF boundary was not a step function. Therefore, it was modeled as a linear ramp function. The subvoxel position of the cord edge was thus estimated across each S/I row of the 5 × 5 grid, and was assumed to be linear across this small span. Points on the interface within the 5 × 5 grid were also used to automatically define the next (inferior) seed point so that the entire process was repeated along the cord, resulting in automated subvoxel characterization of in-plane SC motion.

Cord motion in the A/P direction was characterized from the second cervical (C2) to the second thoracic (T2)

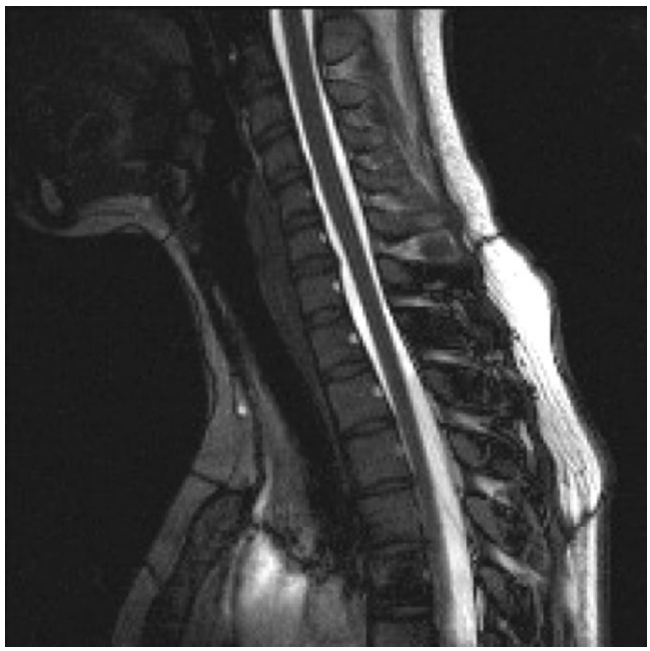

FIG. 1. Image from a single 3.0-mm-thick sagittal slice centered on the midline of the SC and reconstructed from data at a single phase of the cardiac cycle. Good contrast between the cord and CSF was achieved with an in-plane resolution of 1.04 × 1.04 mm^2 over a 200 × 200 mm^2 FOV centered at the level of the C7 vertebra. Using a cardiac-gated, gradient-echo, turbo-FLASH imaging sequence, 24 such images were obtained at different phases of the cardiac cycle, enabling measurement of A/P SC motion.

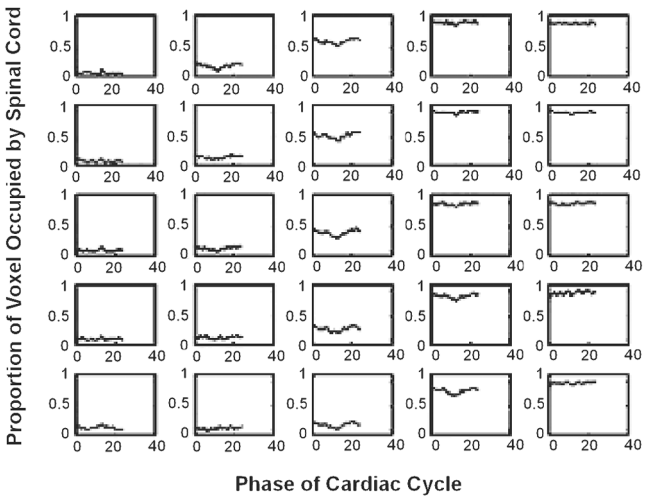

FIG. 2. Time-variant signal intensities of voxels in a 5 × 5 grid centered at the cord/CSF interface at a single S/I position. The signal intensities have been normalized to a value of zero within the CSF and a value of one within the SC. Voxels along the cord/CSF interface have intermediate values, and the values change in time with the motion of the SC.

SC segment. The shape and curvature of the subject's SC relative to the spinal canal resulted in minor variations in how far the cord motion data could be analyzed in the inferior direction. Displacement was measured along the cord in 3-mm S/I increments; however, to reduce the amount of graphical data, it was binned into 5-mm segments before the motion of each subject (Fig. 3) was graphed by combining and averaging motion across all subjects ($N = 9$), those with straight SCs ($N = 5$), and those with curved SCs ($N = 4$). Graphs of R/L SC motion were generated for each subject using a similar procedure before the data were averaged across all subjects ($N = 6$), as well those with straight ($N = 4$) or curved ($N = 2$) SCs. However, due to the variability in SC curvature, slightly different S/I sections of cord were analyzed for each subject.

Principal Components Analysis (PCA) of A/P SC Motion

Consistent features of A/P SC motion were determined by compiling all of the motion data (i.e., every S/I position of every subject) into a single matrix, *M*, to which a singular value decomposition (SVD) was applied. This decomposition demonstrates the eigenvectors and eigenvalues of the covariance matrix of *M*, and reveals its principal components (28).

RESULTS

A/P SC Motion

A/P motion of the cervical and upper thoracic SC was observed in all but one subject, whose data were eliminated due to bulk movement during the imaging session. The timing of the motion was consistent both within and across subjects, whereas the magnitude of motion varied between subjects and with the S/I position along the cords of individual subjects. A plot of typical motion data (Fig. 3) illustrates that the SC moves as a function of the cardiac cycle, and that this motion varies with S/I cord position. Similar motion characteristics of adjacent S/I positions demonstrate the oscillatory pattern of motion along the cord. In Fig. 3, peak cord displacement (i.e., the largest displacement of the cord from its position at peripheral systole) was observed to be 0.44 mm in the anterior direction, a typical value, though slightly lower than the average peak displacement across all nine subjects (0.60 ± 0.34 mm, mean ± SD).

In general, the magnitude of A/P motion was lower and there was less cross-subject variability in the upper cervical SC than in the lower cervical or upper thoracic regions. An apparent dependence of spinal curvature on the amplitude of cord motion was also noted. On average, the five subjects with straight SCs exhibited larger peak A/P motion (0.72 ± 0.33 mm) than the four with curved SCs (0.46 ± 0.32 mm).

R/L SC Motion

Motion of the cervical and upper thoracic SC was observed in the R/L direction for six of the 10 volunteers studied, although the magnitude of this motion was consistently smaller than that observed in the A/P direction. Two subjects were eliminated due to movement between scans, and two were eliminated because severe A/P cord curvature made it impossible to acquire adequate midline coronal images of the cord. In most cases the magnitude of R/L motion was ≤0.10 mm, and the average peak displacement across all six subjects was 0.17 ± 0.09 mm (approximately 1/3 of the average A/P peak displacement).

Analysis of the data grouped according to whether the spine was curved or straight demonstrated that there was no significant difference in R/L motion between the two groups. The cross-subject average of peak R/L displacement of the four subjects with straight SCs was found to be 0.17 ± 0.11 mm, compared to 0.16 ± 0.04 mm for the two subjects with curved SCs.

PCA of SC Motion

After the principal components of SC motion in the A/P direction were calculated, subsets of these were fit to ex-

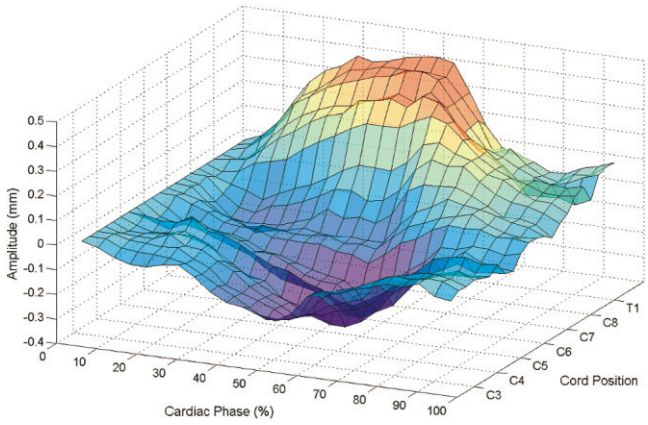

FIG. 3. Typical A/P SC displacement as a function of S/I cord position (every 5 mm) and phase of the cardiac cycle in a single subject. Anterior and posterior displacements are indicated by positive and negative amplitudes, respectively.

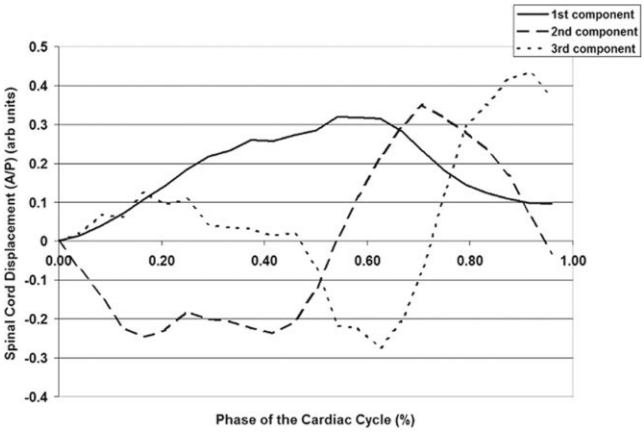

FIG. 4. The first three principal components of SC motion in the A/P direction. These were determined from all measures of the A/P SC motion, at all S/I locations along the cervical SC, across all subjects.

perimentally measured cord motion data by means of a GLM approach. It was observed that using the first three principal components (Fig. 4) was sufficient to estimate the measured motion time courses of all subjects to within the estimated precision of the data. Therefore, the A/P cord motion of each volunteer was modeled from a linear combination of the three principal components, as shown in Fig. 5a. The difference between the modeled and experimental data from Fig. 3 is plotted in Fig. 5b, where the maximum residual is 0.09 mm. The correlation between the estimates and measurements demonstrates the ability to model A/P SC motion from the first three principal components.

DISCUSSION

In the present study, measurements of SC motion were based on the effects of tissue signal averaging, allowing for direct measurement of SC displacement (direction and magnitude of motion). One theoretical limitation of this method is the inability to isolate the three directional components of motion (S/I, A/P, and R/L). Due to the shape and composition of the SC, it is possible for motion in the A/P direction to generate signal intensity changes that erroneously indicate R/L motion, and vice versa. However, the observed motion in the A/P direction was significantly larger than the R/L motion for every subject, indicating that these effects are negligible, and supporting previous observations (19) that SC oscillations are more common in the A/P than the R/L direction. The estimated precision of the results, as indicated by the subtle motion detected in the R/L direction, is $\leq$0.10 mm.

The magnitude of SC motion was found to vary considerably across subjects in both the A/P and R/L directions, with some subjects exhibiting little motion in either direction. This is consistent with observations from a study of a canine model (20), in which motion occurred in only half of the animals and varied considerably among the others. In a human study, integration of cord velocity data (from phase-contrast methods) resulted in an estimated peak cervical cord displacement of 0.4–0.5 mm in the S/I direction (29). Therefore, the present findings (0.60 $\pm$ 0.34 mm and 0.17 $\pm$ 0.09 mm in the A/P and R/L directions, respectively) establish that magnitudes of A/P SC motion commonly meet or exceed those of S/I motion, and suggest that both A/P and S/I motion have significant effects on diffusion and functional MRI methods. Results from the present study suggest that the magnitude of cord motion may be correlated with spinal curvature; however, due to the limited sample size, further investigation is required to test the significance of this correlation.

The effects of S/I cord motion on diffusion imaging in the SC were recently confirmed (17,18), establishing that timing of data acquisition is an important factor for SC DWI and DTI. Empirical data show that the effects of cord motion can be reduced by acquiring data 400 ms following the peripheral pulse (17,18), a finding elucidated by the present cord motion data. Figure 3 shows that although it is never static, cord motion is minimal during the interval spanning 40–60% of the cardiac cycle (i.e., 400–600 ms

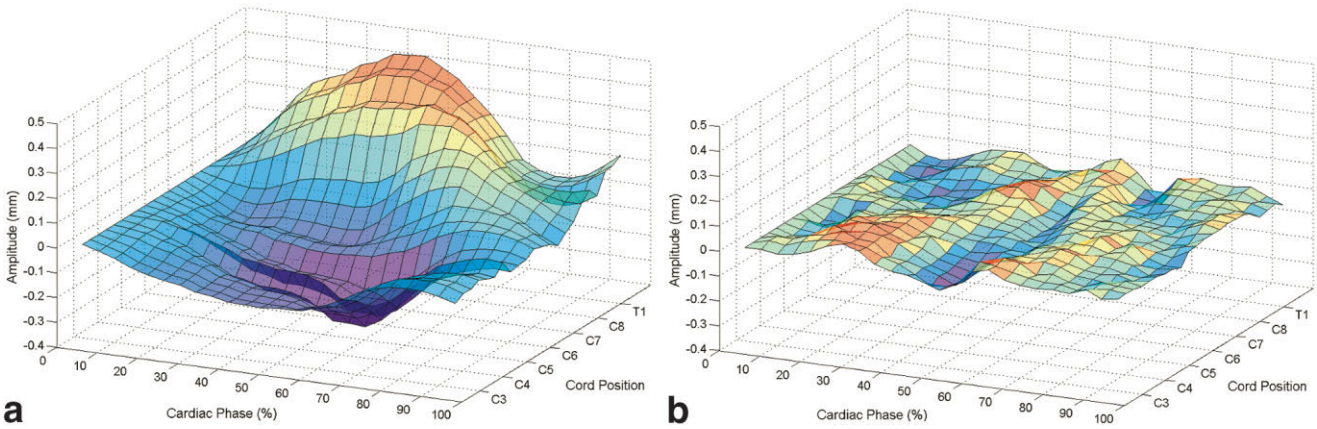

FIG. 5. **a:** A/P SC displacement, modeled with the three principal components of motion, as a function of S/I cord position (every 5 mm) and phase of the cardiac cycle (same subject for whom experimental data are shown in Fig. 3). **b:** Residual between the modeled and experimental data. The significant agreement between the two (the maximum residual in this case is 0.09 mm) indicates that three principal components are sufficient to model A/P SC motion in relation to cardiac activity.

following the peripheral pulse, assuming a cardiac rate of 60 beats per minute). Given that diffusion data are thought to be significantly influenced by S/I SC motion of comparable magnitude (29,17,18), it follows that A/P motion during the effective diffusion time contributes to signal reduction, overestimated diffusion coefficients, and misaligned directional anisotropy.

The regular pattern of cord motion and consistent periods of reduced cord velocity relative to cardiac activity also explain why cardiac-gated acquisitions improve spinal fMRI (27). However, because there is no quiescent period during which the cord is motionless, cardiac gating alone is not expected to be fully effective at countering the effects of SC motion. Another approach has recently shown that both the sensitivity and reliability of spinal fMRI data are enhanced by including traces of the peripheral pulse in a GLM analysis (11), demonstrating that cardiac-related motion presents a significant source of error in spinal fMRI. The results of the present study validate that a large component of this error can be attributed to SC motion.

CONCLUSIONS

In the current study we observed that the cervical SC oscillates in a predictable manner relative to the cardiac cycle. This motion was observed in both the A/P and R/L directions, although the magnitude varied with S/I cord position and across subjects. Motion in the A/P direction is more significant than in the R/L direction, and exceeds previously reported estimates of S/I motion. The three principal components of average A/P cord motion were determined, and the SC motion of individuals was successfully modeled. It is expected that implementation of these principal components in a GLM analysis will enhance the sensitivity and reliability of spinal fMRI, and potentially improve DTI, angiography, and spectroscopy of the SC.

ACKNOWLEDGMENTS

We thank Sharon David for technical assistance and Diana Hsiang for supplementary data analysis and project input.

REFERENCES

1. Weiller C, May A, Sach M, Buhmann C, Rijntjes M. Role of functional imaging in neurological disorders. J Magn Reson Imaging 2006;23:840–850.
2. Sundgren PC, Dong Q, Gomez-Hassan D, Mukherji SK, Maly P, Welsh R. Diffusion tensor imaging of the brain: review of clinical applications. Neuroradiology 2004;46:339–350.
3. Yoshizawa T, Nose T, Moore GJ, Sillerud LO. Functional magnetic resonance imaging of motor activation in the human cervical spinal cord. Neuroimage 1996;4(3 Pt 1):174–182.
4. Stroman PW, Nance PW, Ryner LN. BOLD MRI of the human cervical spinal cord at 3 tesla. Magn Reson Med 1999;42:571–576.
5. Madi S, Flanders AE, Vinitski S, Herbison GJ, Nissanov J. Functional MR imaging of the human cervical spinal cord. AJNR Am J Neuroradiol 2001;22:1768–1774.
6. Backes WH, Mess WH, Wilmink JT. Functional MR imaging of the cervical spinal cord by use of median nerve stimulation and fist clenching. AJNR Am J Neuroradiol 2001;22:1854–1859.
7. Komisaruk BR, Mosier KM, Liu WC, Criminale C, Zaborszky L, Whipple B, Kalnin A. Functional localization of brainstem and cervical spinal cord nuclei in humans with fMRI. AJNR Am J Neuroradiol 2002;23:609–617.
8. Wilmink JT, Backes WH, Mess WH. Functional MRI of the spinal cord: will it solve the puzzle of pain? JBR-BTR 2003;86:293–294.
9. Stroman PW, Krause V, Malisza KL, Frankenstein UN, Tomanek B. Extravascular proton-density changes as a non-BOLD component of contrast in fMRI of the human spinal cord. Magn Reson Med 2002;48:122–127.
10. Stroman PW, Kornelsen J, Lawrence J. An improved method for spinal functional MRI with large volume coverage of the spinal cord. J Magn Reson Imaging 2005;21:520–526.
11. Stroman PW. Discrimination of errors from neuronal activity in functional MRI of the human spinal cord by means of general linear model analysis. Magn Reson Med 2006;452–456.
12. Stroman PW, Tomanek B, Krause V, Frankenstein UN, Malisza KL. Mapping of neuronal function in the healthy and injured human spinal cord with spinal fMRI. Neuroimage 2002;17:1854–1860.
13. Stroman PW, Kornelsen J, Bergman A, Krause V, Ethans K, Malisza KL, Tomanek B. Non-invasive assessment of the injured human spinal cord by means of functional magnetic resonance imaging. Spinal Cord 2004;42:59–66.
14. Bergman A, Leblanc C, Stroman PW. Spinal fMRI of multiple sclerosis: comparison of signal intensity changes with healthy controls. In: Proceedings of the 12th Annual Meeting of ISMRM, Kyoto, Japan, 2004 (Abstract 1035).
15. Wheeler-Kingshott CA, Hickman SJ, Parker GJ, Ciccarelli O, Symms MR, Miller DH, Barker GJ. Investigating cervical spinal cord structure using axial diffusion tensor imaging. Neuroimage 2002;16:93–102.
16. Stroman PW. Magnetic resonance imaging of neuronal function in the spinal cord: spinal FMRI. Clin Med Res 2005;3:146–156.
17. Kharbanda HS, Alsop DC, Anderson AW, Filardo G, Hackney DB. Effects of cord motion on diffusion imaging of the spinal cord. Magn Reson Med 2006;56:334–339.
18. Summers P, Staempfli P, Jaermann T, Kwiecinski S, Kollias S. A preliminary study of the effects of trigger timing on diffusion tensor imaging of the human spinal cord. AJNR Am J Neuroradiol 2006;27:1952–1961.
19. Jokich PM, Rubin JM, Dohrmann GJ. Intraoperative ultrasonic evaluation of spinal cord motion. J Neurosurg 1984;60:707–711.
20. Matsuzaki H, Wakabayashi K, Ishihara K, Ishikawa H, Kawabata H, Onomura T. The origin and significance of spinal cord pulsation. Spinal Cord 1996;34:422–426.
21. Feinberg DA, Mark AS. Human brain motion and cerebrospinal fluid circulation demonstrated with MR velocity imaging. Radiology 1987;163:793–799.
22. Enzmann DR, Pelc NJ. Brain motion: measurement with phase-contrast MR imaging. Radiology 1992;185:653–660.
23. Kohgo H, Isoda H, Takeda H, Inagawa S, Sugiyama K, Yamashita S, Sakahara H. Visualization of spinal cord motion associated with the cardiac pulse by tagged magnetic resonance imaging with particle image velocimetry software. J Comput Assist Tomogr 2006;30:111–115.
24. Levy LM, Di CG, McCullough DC, Dwyer AJ, Johnson DL, Yang SS. Fixed spinal cord: diagnosis with MR imaging. Radiology 1988;169:773–778.
25. Tanaka H, Sakurai K, Kashiwagi N, Fujita N, Hirabuki N, Inaba F, Harada K, Nakamura H. Transition of the craniocaudal velocity of the spinal cord: from cervical segment to lumbar enlargement. Invest Radiol 1998;33:141–145.
26. Enzmann DR, Pelc NJ. Normal flow patterns of intracranial and spinal cerebrospinal fluid defined with phase-contrast cine MR imaging. Radiology 1991;178:467–474.
27. Brooks J, Robson M, Schweinhardt P, Wise R, Tracey I. Functional magnetic resonance imaging (fMRI) of the spinal cord: a methodological study. In: Proceedings of the 23rd Annual Meeting of the American Pain Society, Vancouver, Canada, 2004. p 667.
28. Golub GH, Van Loan CF. Matrix computation. Baltimore: Johns Hopkins University Press; 1996.
29. Mikulis DJ, Wood ML, Zerdoner OA, Poncelet BP. Oscillatory motion of the normal cervical spinal cord. Radiology 1994;192:117–121.